Manuscript prepared for Geosci. Model Dev.
with version 5.0 of the LaTeX class copernicus.cls.
Date: 30 June 2014

Simulations of direct and reflected waves trajectories for ground-based GNSS-R experiments

N. Roussel[1,2], F. Frappart[1,2], G. Ramillien[1,2], C. Desjardins[1,2,3,4], P. Gegout[1,2], F. Pérosanz[1,2,4], and R. Biancale[1,2,4]

[1]Université de Toulouse, CNRS, IRD, GET-OMP, Toulouse, France
[2]Groupe de Recherche en Géodésie Spatiale, Toulouse, France
[3]Collecte Localisation Satellites, Ramonville Saint Agne, France
[4]Centre National d'Etudes Spatiales, Toulouse, France

Correspondence to: N. Roussel
(nicolas.roussel@get.obs-mip.fr)

Abstract. The detection of Global Navigation Satellite System (GNSS) signals that are reflected off the surface, together with the reception of direct GNSS signals offers a unique opportunity to monitor water level variations over land and ocean. The time delay between the reception of the direct and the reflected signal gives access to the altitude of the receiver over the reflecting surface. The field of view of the receiver is highly dependent on both the orbits of the GNSS satellites and the configuration of the study site geometries. A simulator has been developed to determine the accurate location of the reflection points on the surface by modelling the trajectories of GNSS electromagnetic waves that are reflected on the surface of the Earth. Only the geometric problem have been considered using a specular reflection assumption. The orbit of the GNSS constellations satellite (mainly GPS, GLONASS and Galileo), and the position of a fixed receiver are used as input. Four different simulation modes are proposed depending on the choice of the Earth surface model (plane, sphere or ellipsoid) and the consideration of topography likely to cause masking effects. Atmospheric delay effects derived from adaptive mapping functions are also taken into account. This simulator was developed to determine where the GNSS-R receivers should be located to monitor efficiently a given study area. In this study, two test sites were considered. The first one at the top of the 65 meters Cordouan lighthouse in the Gironde estuary, France, and the second one in the shore of the Geneva lake (50 meters above the reflecting surface). This site is hidden by mountains in the south (orthometric altitude up to 2000 m), and overlooking the lake in the north (orthometric altitude of 370 m). For this second test site configuration, reflections occur until 570 m from the receiver. The planimetric (arc length) differences (resp. altimetric difference as WGS84 ellipsoid height) between the positions of the specular reflection points obtained considering the Earth's surface as a sphere or as an ellipsoid were found to be on average 64 cm (resp. 13 cm) for satellites elevation angle greater than 10° and 120 cm (resp. 19 cm) for satellite elevation angle between 5° and 10°. The altimetric and planimetric differences between the plane and sphere approximations are on average below 2 mm for satellites elevation angle greater than 10° and below 6 mm for satellite elevation angle between 5° and 10°. The simulations highlight the importance of the Digital Elevation Model (DEM) integration: average planimetric differences (resp. altimetric) with and without integrating the DEM (with respect to the sphere approximation) were found to be about 91 m (resp. 40 m) with the minimum elevation angle equal to 5°. The correction of the tropospheric effects on the signal leads to planimetric differences (resp. altimetric) about 18 m (resp. 6 cm) maximum for a 50-meter receiver height above the reflecting surface whereas the maximum is 2.9 m (resp. 7 mm) for a 5-meter receiver height above the reflecting surface. These errors deeply increase with the receiver height above the reflecting surface. By setting it to 300 m, the planimetric errors reach 116 m and altimetric errors reach 32 cm for satellite elevation angle lower than 10°. The tests performed with the simulator presented in this paper highlight the importance of the choice of the Earth representation and also the non-negligible effect of the troposphere on the specular reflection points positions. Various outputs (time-varying reflection point coordinates, satellites positions and ground paths, wave trajectories, first Fresnel zones, etc.) are provided either as text or KML files for visualizing with Google Earth.

1 Introduction

The Global Navigation Satellite System (GNSS), which includes the American GPS, the Russian GLONASS, and the European Galileo (which is getting more and more denser) uses L-band microwave signals to provide accurate 3-D positioning on any point of the Earth surface or close to it. Along with the space segment development, the processing techniques have also improved considerably, with a better consideration of the various sources of error in the processing. Among them, multipaths still remain a major problem, and the mitigation of their influence has been widely investigated (Bilich A.L. , 2004). ESA (European Space Agency) first proposed the idea of taking advantage of the multipaths phenomenon in order to assess different parameters of the reflecting surface (Martin-Neira M. , 1993). This opportunistic remote sensing technique, known as GNSS-Reflectometry (GNSS-R), is based on the analysis of the electromagnetic signals emitted continuously by the GNSS satellites and detected by a receiver after reflection on the Earth's surface. Several parameters of the Earth surface can be retrieved either using the time-delay between the signals received by the upper (direct signal) and the lower (reflected signal) antennas, or by analyzing the waveforms (temporal evolution of the signal power) corresponding to the reflected signal. This technique offers a wide-range of applications in Earth sciences. The time-delay can be interpreted in terms of altimetry as the difference of height between the receiver and the surface. Temporal variations of sea (Lowe S.T. et al. , 2002; Ruffini G. et al. , 2004; Löfgren J.S. et al. , 2011; Semmling A.M. et al. , 2011; Rius A. et al. , 2012) and lakes level (Treuhaft P. et al. , 2004; Helm A. , 2008) were recorded with an accuracy of a few centimeters using in situ and airborne antennas. Surface roughness can be estimated from the analysis of the Delay-Doppler Maps (DDM) derived from the waveforms of the reflected signals. They can be related to parameters such as soil moisture (Katzberg S. et al. , 2006; Rodriguez-Alvarez N. et al. , 2009, 2011) over land, or wave heights and wind speed (Komjathy A. et al. , 2000; Zavorotny A.U. et al. , 2000; Rius A. et al. , 2002; Soulat F. et al. , 2004) over the ocean, or ice properties (Gleason S. , 2006; Cardellach E. et al. , 2012). GNSS-R technique presents two main advantages: (1) a dense spatial and temporal coverage, not only limited to a single measurement point or a non repetitive transect as using classical GNSS buoys, (2) a guarantee of service for the next decades (because of the strategic role played by these systems). GNSS-R altimetric accuracy is today at the level of few centimeters. But this technique will benefit, in the future, from improved processing technique and from the densification of the GNSS constellation. The commonly-used GNSS-R system consist of two antennas (figure 1): the first one is right-hand circular polarized (RHCP) and zenith-facing to receive the direct waves. The second one, left-hand circular polarized (LHCP) and nadir-facing to receive the reflected waves. These reflected waves will mostly change their polarization from RCHP to LHCP by reflecting at near-normal incidence. The reflected signals have an additional path delay with respect to the direct ones. The analysis of the path difference between these direct and reflected signals is used to estimate the relative height difference between the two antennas. In order to anticipate the impact of the geometric configuration of the experiment, a simulator has been developed to estimate the positions of reflection points using a specular reflection point assumption. Four different methods were implemented: approximating the Earth's surface as a plane, as a sphere, as an ellipsoid or integrating a Digital Elevation Model (DEM). In addition, the signal bending due to the neutral part of atmosphere is taken into account using the Adaptive Mapping Functions (AMF) from Gegout et al. (2011) and made available by GRGS (Groupe de Recherche en Géodésie Spatiale). Simulations were performed for different configurations: variations in the reflectometer height, mask effects due to terrain, satellite network geometry.

This article is composed by three main parts following the logical structure of the figure 2. The first part presents the datasets used for initiating simulations, the second one concerns the methodologies for the determination of the reflection points while the last one deals with the simulator performances and simulation results.

Design of the simulator

The simulator has been developed in the GNU R language, generally used for data treatment and statistical analysis. A user manual and a description of the R language can be found on the website http://www.r-project.org/. The main interest of such a language remains in that it is distributed under GNU GPL license which does R routines an open source program, available on various platforms (i.e. GNU/Linux, FreeBSD, NetBSD, OpenBSD, Mac OS and Windows).
The simulator is composed by three main blocks (figure 2): an input block which contains the different elements mandatory for the processing; a processing block where the user can choose which algorithm to be used, and an output block containing the different results of the simulation.

As inputs, this simulator requires the receiver coordinates, the satellite ephemeris and a set of optional environmental parameters such as a DEM in order to take the possible masking of the terrestrial topography into account, as well as adaptive mapping functions to integrate atmospheric delays and bending effects.

As outputs, the simulator provides the time-varying reflection point coordinates, but also various KML files (*Keyhole Markup Language* - standard format used by Google Earth) such as satellites positions and ground paths, waves trajectories and Fresnel first surfaces which can be opened using the Google Earth visualization tool.

2 Datasets

2.1 GNSS orbit parameters

The simulations are based on the determination of the positions of the specular reflection points, once the receiver and the satellites positions are known. Satellites coordinates can be obtained from the International GNSS Service (IGS) ephemeris final products which provide GNSS orbit and clock offset data with a temporal resolution of 15 minutes in the SP3 format for the past epochs, or derived from the Keplerian parameters (semi-major axis, inclination, and argument of perigee) to predict GNSS satellite positions. Ephemeris products are available on the IGS website: http://igs.org/ and Keplerian parameters e.g. on: http://www.navcen.uscg.gov

2.2 Radio-electric mask

Simulations are performed for a given receiver position in the WGS84 coordinates system and height above the ground. It is possible to apply an elevation or azimuthal angles mask to the simulations to avoid satellites with low elevation angle for instance. The elevation angle mask commonly used is set to 10° min and 90° max and no mask is set in azimuth.

2.3 SRTM Digital Elevation Model

The most realistic simulation needs the integration of a Digital Elevation Model (DEM) in order not to only take the possible masking of satellites into account, but to get more accurate and exact positions of the specular reflection points as well. The hole-filled version 4 of the Shuttle Radar Topography Mission (SRTM) DEM, with a spatial resolution of 90 m at the equator is used (Jarvis J. et al. , 2008). The altitudes are given with reference to the EGM96 geoid model. Uncertainty on altitude is around 16 m over mountainous areas (Rodriguez E. et al. , 2005). It is made available by files of 5° x 5° for land areas between 60°N and 60°S by the Consortium for Spatial Information (CGIAR-CSI): http://srtm.csi.cgiar.org/.

2.4 Earth Gravitational Model EGM96

In order to be able to convert between ellipsoidal heights (with respect to the WGS84 ellipsoid) and altitudes (with respect to the EGM96 geoid model) when producing KML files or when integrating a DEM, the knowledge of the geoid undulation is mandatory. In this study, we interpolate a 15 x 15-Minute Geoid Undulation Grid file derived from EGM96 model in a tide-free system released by the U.S. National Geospatial-Intelligence Agency (NGA) EGM Development Team:

http://earth-info.nga.mil/GandG/wgs84/gravitymod/. The error on the interpolation is lower than 2 cm (NASA and NIMA , 1998).

2.5 Adaptive Mapping Functions

The neutral atmosphere bends the propagation path of the GNSS signal and retards the speed of propagation. The range between the satellite and the tracking site is neither the geometric distance nor the length of the propagation path, but the radio range of the propagation path (Marini J.W. , 1972).

For GNSS-R measurements, the tropospheric effects induced by the neutral part of the atmosphere are an important source of error. Indeed, GNSS-R measurements are often done at low elevation angle where the bending effects are maximal. Accurate models have to be used to mitigate signal speed decrease and path bending. It is commonly accepted to model tropospheric delays by calculating the zenith tropospheric delay and obtaining the slant tropospheric delays with a mapping function. New mapping functions have been developed in the 2000's (Boehm J. et al , 2006; Niell A. , 2001) and significantly improve the geodetic positioning. Although modern mapping functions like VMF1 (Boehm J. et al , 2006b) and GPT2/VMF1 (Lagler K. et al. , 2013) are derived from Numerical Weather Models (NWM), most of these mapping functions ignore the azimuth dependency which is usually introduced by two horizontal gradient parameters - in north-south and east-west directions - estimated directly from observations (Chen G. et al. , 1997). More recently, the use of ray-traced delays through NWM directly at observation level has shown an improvement on geodetic results (Hobiger T. et al , 2008; Nafisi V. et al , 2012; Zus F. et al , 2012). The Adaptive Mapping Functions (AMF) are designed to fit the most information available in NWM - especially the azimuth dependency - preserving the classical mapping function strategy. AMF are thus used to approximate thousands of atmospheric ray-traced delays using a few tens of coefficients with millimetre accuracy at low elevation (Gegout P. et al. , 2011). AMF have a classical form with terms which are function of the elevation. But, they also include coefficients which depend on the azimuth to represent the azimuthal dependency of ray-traced delays. In addition, AMF are suitable to adapt to complex weather by changing the truncation of the successive fractions. Therefore, the AMF are especially suited to correct propagation of low elevation GNSS-R signals. In our study we use AMF directly provided by GRGS (Groupe de Recherche en Géodésie Spatiale) and computed following (Gegout P. et al. , 2011).

2.6 Data used for assessment

In order to assess the simulator performance and the ocean tide influence on the positions of the reflection points estimated at an offshore experimental site located at the top of the Cordouan lighthouse (45°35'11"N ; 1°10'24"W), we use 24 hours of REFMAR (*Réseau de Référence des Observations Marégraphiques*) tide gauge observations, with a sampling frequency of 5 minutes. The tide gauge records of the station of Royan (45°37'14.07"N;1°01'40.12", located

12 km from the lighthouse) are the property of MEDDE (Ministère de l'Ecologie, du Développement Durable et de l'Energie), and they are available on the REFMAR website (http://refmar.shom.fr)).

3 Methodology : determination of the positions of reflection points

The difference of phase between the two antennas (A-RHCP and B-LHCP on figure 1) at an epoch t for the i^{th} GNSS satellite can be seen as a classical single difference between two receivers used for relative positioning as follows :

$$\lambda\Delta\phi^i_{AB}(t) = \Delta\delta^i_{AB}(t) - \lambda\Delta N^i_{AB} - c\Delta t_{AB} \quad (1)$$

where λ is the wavelength of the GNSS wavelength carrier, $\Delta\phi^i_{AB}$ the measured carrier phase difference between the direct and received signals expressed in cycles, $\Delta\delta^i_{AB}$ the difference in distance between the direct and received signals, ΔN^i_{AB} is the difference of phase ambiguity between the direct and received signals, c the speed of light in vacuum, Δt_{AB} the receivers clock bias difference. As the baseline between the two receivers is short (a few centimeters to a few tenth of centimeters), and in the case of low altitude of the receivers, both tropospheric and ionospheric effects are neglected due to the spatial resolution of the current atmospheric and ionospheric models. Besides, when both antennas are connected to same receiver, the receiver clock bias difference is also cancelled out. In this study, we only consider the difference in distance between direct and reflected signals as illustrated in figure 1.

The processing block contains four algorithms for determining the positions of the specular reflection points: the first considering the Earth as a local plane in the vicinity of the reflection point, the second as a local sphere, the third as an ellipsoid (corresponding to the WGS84 ellipsoid adjusted to the position of the receiver on the ground), and the last one uses an ellipsoid approximation and takes the Earth's topography into account: see figure 3. As it will be discussed in the subsection 4.1, the three algorithms have different characteristics, in terms of calculation time and accuracy of the positions determination.

All of them are based on iterative approaches to solve the Snell-Descartes law for reflection: the unique assumption is that the angle of incidence is equal to the angle of reflection on a plane interface separating two half-space media (a locally planar approximation is adopted when the surface is not everywhere planar). In the plane, sphere and ellipsoid approximations, the specular reflection point of a given satellite is contained within the plane defined by the satellite, the receiver and the center of the Earth. With regards to the DEM integration, reflection can occur everywhere. In order to be able to compare the specular reflection points positions obtained by integrating a DEM, and to simplify the problem, we will only consider the reflections occurring within the plane, even while integrating a DEM.

3.1 Local plane reflection approximation

Let us consider the projection of the receiver $R0$ on an osculating sphere approximation (figure 3). We define the local plane P as the plane tangent to the sphere at $R0$. Let $T0$ be the projection of the satellite on P and R' the symmetry of $R0$ relative to P. We look for the positions of the specular reflection points on P. Considering the Thales theorem in the triangles $R'SR0$ and $STT0$, we have (see figure 3):

$$\frac{X_S}{(X_{T0} - x_S)} = \frac{h}{H} \quad (2)$$

And so:

$$X_S = \frac{hX_{T0}}{X_{T0} + h} \quad (3)$$

3.2 Local sphere reflection approximation

J. Kostelecky and C. Wagner already suggested an algorithm to retrieve the specular reflection point positions by approximating the Earth as a sphere in (Kostelecky J. et al. , 2005; Wagner C., Klokocnik J. , 2003). Their algorithm is based on an optimized iterative scheme which is equivalent to make the position of a fictive specular point vary until verifying the first law of Snell-Descartes. A similar approach will be used in this paper in the subsection 3.3 with the ellipsoid approximation. Here we chose to adopt a more analytical algorithm, first proposed by (Helm A. , 2008). In order to validate this algorithm, comparisons between it and the iterative one developed for the ellipsoid approach will be done, by setting the minor and major axis of the ellipsoid equal to the sphere radius (see part 4.2.1).

Let us consider the vertical plane formed by the transmitter (GNSS) satellite (T), the receiver (R) and O, the centre of the Earth (figure 4). We assume that the specular reflection point (S) will be included in that plane. Let us consider the following orthonormal reference systems of coordinates:

- $(O, X, Y, Z)_{R1}$: WGS84 Cartesian system (NIMA , 1997), with O the centre of the Earth. WGS84 has Z polar and X,Y equatorial. The receiver and transmitter coordinates are known in this system.
- $(O, x, y)_{R2}$: a local two-dimensional system, obtained by the rotation of the (O,X,Y,Z) system around the Z axis, in such a way that x_r = 0.
- $(S, x', y')_{R3}$: a local two-dimensional system, obtained by a rotation around the z axis and a r_E translation of the (O,x,y) system in such a way that x' and the local vertical are colinear, and that the system origin coincides with the specular reflection point S.

If H is the height of the receiver above the ground, the position of the receiver is:

$$\boldsymbol{r_r} = \begin{pmatrix} x_r \\ y_r \end{pmatrix}_{R2} = \begin{pmatrix} 0 \\ r_E + H \end{pmatrix}_{R2} \quad (4)$$

with

$$r_E = \frac{a^2 b}{a cos(\varphi)^2 + b sin(\varphi)^2} \quad (5)$$

the Gaussian radius of curvature at the latitude of the receiver φ_r.

a being the semi-major axis of the WGS84 ellipsoid, and b the semi-major axis of the WGS84 ellipsoid.

The position of the GNSS satellite transmitter considering ε the elevation angle of the satellite (considering zenith angle reckoned from the ellipsoidal normal direction) and τ the angle $\widehat{RTO}$ is given by:

$$\boldsymbol{r_t} = \begin{pmatrix} x_t \\ y_t \end{pmatrix}_{R2} = \begin{pmatrix} r_t cos(\varepsilon + \tau) \\ r_t sin(\varepsilon + \tau) \end{pmatrix}_{R2} \quad (6)$$

Using the trigonometric sine formula in the R-T-0 triangle:

$$\frac{sin(\frac{\pi}{2} + \varepsilon)}{r_t} = \frac{sin(\tau)}{r_E + H} \quad (7)$$

We finally obtain:

$$\begin{pmatrix} x_t \\ y_t \end{pmatrix}_{R2} = \begin{pmatrix} r_t cos(\varepsilon)\sqrt{1 - \frac{(r_E+H)^2}{r_t^2} cos^2(\varepsilon)} \\ -(r_E + H) sin(\varepsilon) cos(\vartheta) \\ \\ r_t sin(\varepsilon)\sqrt{1 - \frac{(r_E+H)^2}{r_t^2} cos^2(\varepsilon)} \\ -(r_E + H) cos^2(\vartheta) \end{pmatrix}_{R2} \quad (8)$$

The Snell-Descartes law for reflection can be expressed as the ratios of the coordinates of the receiver and the transmitter in (S, x', y'):

$$\frac{x'_t}{y'_t} = \frac{x'_r}{y'_r} \quad (9)$$

The coordinates in R3 can be derived from the coordinates in (O, x, y) from:

$$\begin{pmatrix} x' \\ y' \end{pmatrix}_{R3} = \begin{pmatrix} cos(\gamma) & sin(\gamma) \\ -sin(\gamma) & cos(\gamma)) \end{pmatrix}_{R3} \begin{pmatrix} x \\ y \end{pmatrix}_{R3} - \begin{pmatrix} r_e \\ 0 \end{pmatrix}_{R3} \quad (10)$$

where γ is the rotation angle between the two systems (figure 4) . So (9) becomes:

$$\begin{aligned} &2(x_t x_r - y_t y_r) sin(\gamma) cos(\gamma) \\ &-(x_t y_r + y_t x_r)(cos^2(\gamma) - sin^2(\gamma)) \\ &-r_E(x_t + x_r) sin(\gamma) + r_e(y_t + y_r) cos(\gamma) = 0 \end{aligned} \quad (11)$$

Following (Helm A. , 2008), we proceed to the substitution $t = tan(\frac{\gamma}{2})$, and (11) becomes:

$$\begin{aligned} 2(x_t x_r - y_t y_r)\frac{2t}{1+t^2}\frac{1-t^2}{1+t^2} - x_t y_r((\frac{1-t^2}{1+t^2})^2 \\ -(\frac{2t}{1+t^2})^2) - r_E \frac{2t}{1+t^2}(x_t + x_r) \\ +r_E \frac{1-t^2}{1+t^2}(y_t + y_r) = 0 \end{aligned} \quad (12)$$

And finally becomes:

$$c_4 t^4 + c_3 t^3 + c_2 t^2 + c1_t^1 + c_0 = 0 \quad (13)$$

with:

$$c_0 = (x_t y_r + y_t x_r) - r_E(y_t + y_r) \quad (14)$$
$$c_1 = -4(x_t x_r - y_t y_r) + 2r_E(x_t + x_r) \quad (15)$$
$$c_2 = -6(x_t y_r + y_r x_r) \quad (16)$$
$$c_3 = 4(x_t x_r - y_t y_r) + 2r_E(x_t + x_r) \quad (17)$$
$$c_4 = (x_t y_r + y_t x_r) + r_E(y_t + y_r) \quad (18)$$

Equation (13) is solved to determine the roots of this polynom using an iterative scheme based on the Newton method (Nocedal J. et al. , 2006).

3.3 Ellipsoid reflection approximation

By knowing the locations of the transmitter and the receiver on the local ellipsoid included in the plane defined by the centre of the Earth, the receiver and the transmitter, let us consider the two normalized anti-incident r_t and scattering r_r vectors.When the Snell-Descartes law is verified, the sum of the two vectors (bisecting vector dr) coincides with the local vertical r_s (figure 5). The determination of the location of the reflection point is based on iterative process proposed earlier by (Gleason S. et al. , 2009), and enhanced with a dichotomy process. Let us consider three points on the ellipsoid:

- $S1$ the projection of the receiver on the ellipsoid
- $S3$ the projection of the transmitter on the ellipsoid
- $S2$ the projection of the middle of $[S1S3]$ on the ellipsoid

We calculate dr, the correction in direction, for each of the three points:

$$\boldsymbol{dr}(t) = \frac{\boldsymbol{r_s}(t) - \boldsymbol{r_r}(t)}{\|\boldsymbol{r_s}(t) - \boldsymbol{r_r}(t)\|} + \frac{\boldsymbol{r_s}(t) - \boldsymbol{r_t}(t)}{\|\boldsymbol{r_s}(t) - \boldsymbol{r_t}(t)\|} \quad (19)$$

We consider then the direction of the correction dr. If the correction is in the satellite direction, the sign is considered as positive, and negative if the correction is in the receiver direction. If the signs of dr_{S1} and dr_{S2} are different, it means

that the specular reflection point is located between $S1$ and $S2$. We thus consider a new iteration with $S1 = S1, S3 = S2$ and $S2$ the projection on the ellipsoid of the middle of the new $S1$ and $S3$ points. We thus eliminate the part between the initial $S2$ and $S3$ points. Else if the signs of dr_{S2} and dr_{S3} are different, we consider a new iteration with $S1 = S2$ and $S3 = S3$ (and $S2$ the projection on the ellipsoid of the middle of the new $S1$ and $S3$ points). The iterative process stops when the difference between incident and reflected angle (with respect to the local vertical) is close to zero with a fixed tolerance of $1e-7°$.

3.4 Ellipsoid reflection approximation combined with a DEM

The two first approaches presented above are well adapted in the case of an isolated receiver, located on the top of a light house, for instance. In most of the cases, the receiver is located on a cliff, a sand dune, or a building overhanging the sea surface or a lake. It can however be really appropriate and necessary to incorporate a Digital Elevation Model (DEM) into the simulations, in order not to only take the mask effects (e.g., a mountain occulting a GNSS satellite) into account, but also to get more accurate and realistic positions of specular reflection points. The method we propose here consists of three steps later detailed in subsections 3.4.1, 3.4.2 and 3.4.3.

1. A "visibility" determination approach to determine if the receiver is in sight of each GNSS satellite.
2. A determination of the specular reflection point position.
3. A "visibility" determination approach to determine if the determined specular point is in sight from both receiver and satellite.

We have to keep in mind that a DEM gives altitudes above a reference geoid. For consistency purpose, the positions of the receiver and the transmitter, and the DEM grid points have all to be in the same reference system. So it is absolutely mandatory to convert the altitudes of the DEM grid points into ellipsoidal heights by adding the geoid undulation. To do so, a global grid from the EGM96 geoid undulation model with respect to the WGS84 ellipsoid was removed from SRTM DEM grid points.

3.4.1 Visibility of the GNSS satellite from the receiver

This algorithm aims to determine the presence of mask between the receiver and the satellite. The visibility of the satellite and of the receiver, both from the specular point will be checked once the potential specular point position will be found.

Let R, S, and T be the locations of the receiver, the specular point and the satellite/transmitter on the ellipsoid. We interpolate the ellipsoidal heights along the path $[TSR]$ with a step equal to the DEM resolution, with a bivariate cubic or bilinear interpolation. Cubic interpolation is used when the gradient is big, linear interpolation otherwise. Tests show millimetric differences between cubic and linear interpolation for flat zones but can reach one meter for mountainous areas. We thus obtain a topographic profile from R to T. For each segment of this topographic profile, we check if it intersects the path $[TR]$. If it does, it means that the satellite is not visible from the receiver. If not, we check the next topographic segment, until reaching the end of the path (i.e. T).

3.4.2 Position of the specular point

Once the satellite visibility from the receiver is confirmed, the next step consists in determining the location of the specular reflection point S along the broken line defined as in subsection 3.4.1. In order to simplify the process, we only consider the specular points located into the plane formed by the satellite, the receiver and the center of the Earth. The algorithm is similar to the one used for the ellipsoid approximation and is based on a dichotomous iterative process.

The segments formed by the points of the 2D DEM (see figure 6) are all considered susceptible to contain a specular reflection point. For each of this segment, we check the sign of the correction to apply for the two extremities of the segment with the same principle that for the ellipsoid approximation (see subsection 3.3), but with a local vertical component defined as the normal of the considered segment. If the signs are equal, no reflection is possible on this segment. Otherwise, we apply the dichotomous iterative method presented in subsection 3.3 until convergence with respect to the tolerance parameter (fixed to $1e-7°$).

3.4.3 Visibility of the determined specular reflection point from the satellite and the receiver

Once the position of the specular reflection point is determined, we check if it is visible from the satellite and the receiver thanks to the algorithm presented in subsection 3.4.1.

3.5 Tropospheric corrections

In order to correct the anisotropy of propagation of radio waves used by the GNSS satellites, we use AMF calculated from the 3-hourly delayed cut-off in model levels computed by the ECMWF (European Centre for Medium-Range Weather Forecasts). AMF tropospheric corrections were computed following (Gegout P. et al. , 2011) and provided by GRGS for this study. Given the geometric specificities of the specular reflection point, two paths have to be checked for propagation error: the first one from the satellite to the surface, and the second from the surface to the receiver. The main steps of the process are the following:

1 We consider the position of the specular reflection point without any correction of the tropospheric errors;

2 We calculate the corrections to apply to this specular point knowing the incident and reflecting angle corresponding to the considered reflection point. We thus obtain a corrected incident angle. Figure 7 shows the correction to apply as a function of the elevation angle;

3 With the corrected incident angle, a corrected position of the specular point is calculated, making the reflecting angle being equal to the corrected incident angle;

4 With the new position of the specular point and to reach a better accuracy of the point position, a second iteration is done calculating the corrections to apply to this new incident angle.

3.5.1 Correction of the satellite-surface path

First and foremost, we solve the parallax problem for the wave emitted by a known GNSS satellite. At first sight, we consider the position of the specular reflection point calculated without any tropospheric correction, given by the algorithm approximating the Earth's shape as a sphere given in paragraph 3.2. We use here AMF calculated from the projection of the receiver on the surface, considering that the AMF planimetric variations are negligible for ground-based observations (i.e. we consider that we can use the same AMF for every specular reflection points, which is valid only if the specular reflection points are less than few tens of kilometres from the receiver and that the specular points lie on an equal-height surface). We thus obtain the corrected incident angle of the incident wave. Considering the law of Snell-Descartes, the reflecting angle must be equal to the corrected incident angle, for the specular reflection point position.

3.5.2 Correction of the surface-receiver path

The aim here is to adjust the surface-receiver path to accommodate for the consequences of angular refraction. With the corrected reflection angle, we can deduce the corrected geometric distance between the reflection point and the receiver, using this time AMF calculated from the receiver, assuming that the AMF altimetric variations are non-negligible (i.e. the part of the troposphere corresponding to the receiver height will have a non-negligible impact on the AMF). Considering the corrected geometric distance between the reflection point and the receiver, the corrected position of the reflection point is obviously determined. It is indeed obtained by intersection between a circle whose radius is equal to the correct geometric distance, and the surface of the Earth assimilated as a sphere, an ellipsoid, or with a DEM, depending on which approximation of the Earth is taken into account.

We iterate the whole process a second time to reach a better accuracy of the reflection point position. In fact, the first corrections were not perfectly exact since calculated from an initially false reflection point position, and the second iteration brings the point closer to the correct position. More iterations are useless (corrections to apply are no significant). Figure 7 shows an example of elevation corrections to apply as a function of the satellite elevations. This figure has been computed from simulations done on a receiver placed on the Geneva Lake shore (46°24'30N" ; 6°43'6"E ; 471m): see subsection 4.1 page 7.

3.6 Footprint size of the reflected signal

The signal power received is mostly due to coherent reflection and most of scattering is coming from the first Fresnel zone (Beckmann P. and Spizzichino A. , 1987). The first Fresnel zone can be described as an ellipse of semi-minor axis (a) and semi-major axis (b) equal to (Larson K.M. and Nievinski F.G. , 2013):

$$r_b = \sqrt{\frac{\lambda h}{sin(\epsilon')} + (\frac{\lambda}{2sin(\epsilon')})^2} \tag{20}$$

$$r_a = \frac{b}{sin(\epsilon')} \tag{21}$$

With λ the wave length (m), h the receiver height (m) and ϵ' the satellite elevation seen from the specular reflection point (rad) (i.e. corresponds to the reflection angle).

4 Simulator performance and results

4.1 Simulation study cases

Simulations and tests of parameters have been performed on two main sites:

- the Cordouan lighthouse (45°35'11"N ; 1°10'24"W), in the Gironde Estuary, France. This lighthouse is about 60 meters high, and it is surrounded by the sea.
- the shore of the Geneva lake (46°24'30N";6°43'6"E). This site is hidden by mountains in the South (orthometric altitude up to 2000 m), and overlooks the lake in the North (orthometric altitude of 370 m).

For both sites, precise GPS and GLONASS ephemeris at a 15-minute time-sampling come from IGS standard products (known as "SP3 orbit").

4.2 Validation of the surface models

Simulations have been performed in the case of the Geneva Lake shore, for a 24-hour experiment, on the 4^{th} october 2012.

4.2.1 Cross-validation between sphere and ellipsoid approximations

Local sphere and ellipsoid approximation algorithms have been compared by putting the ellipsoid semi- major and minor axis equal to the sphere radius. Planimetric and altimetric differences between both are below 6.10^{-5} m for a receiver height above reflecting surface between 5 and 300 m and are then negligible. The two algorithms we compare are totally different: the first is analytical and the second is based on a iterative scheme and both results are very similar, which confirms their validity.

4.2.2 Cross-validation between ellipsoid approximation and DEM integration

The algorithm integrating a DEM has been compared to the ellipsoid approximation algorithm by putting a flat DEM as input (i.e. a DEM with orthometric altitude equal to the geoid undulation). Results for satellite elevation angles above 5° are presented in table 1.

As we can see in table 1, planimetric and altimetric mean differences are subcentimetric for a 5 and 50 m receiver height and centimetric for a 300 m receiver height. However, some punctual planimetric differences reach 70 cm in the worst conditions (reflection occurring at 3408 m from the receiver corresponding to a satellite with a low elevation angle), which can be explained with the chosen tolerance parameters but mainly because due to the DEM resolution, the algorithm taking a DEM into account approximating the ellipsoid as a broken straight line, causing inaccuracies. For a 50 m receiver height, planimetric differences are below 10 cm (reflections occurring until 573 meters from the receiver). With regards to the altimetric differences, even for reflections occurring far from the receiver, the differences are negligible (submillimetric).

4.3 Simulator outputs

4.3.1 Plot of the specular reflection points and recap text files

The simulator provides the position of the reflection points estimated during the selected time period of the simulation for each satellite, with a time-step of 15 minutes. These successive positions are mapped gradually on a pop-up window of the R software and their coordinates are contained in a text file which summarizes the different selected parameters of the simulation, as well.

4.3.2 KML files

The coordinates of the simulated specular reflection points are provided as KML files too: it is possible to use Google Earth to visualize them. This allows us to use the Google Earth time-selection cursor to visualize the simulation results either at every pre-step Δt (i.e., every 15 minutes), or cumulated over longer timer period $\Delta T = \sum_{i=1}^{n} \Delta t_i$. The different KML files created at the end of each simulation and viewable in Google Earth are the following:

- Positions of the specular reflection points
- Positions of the receiver and satellites
- Ground paths of the satellites
- Direct and reflected waves
- First Fresnel surface

4.4 Results

4.4.1 Cordouan lighthouse

Outputs

Examples of visualization of outputs for simulations in the case of the Cordouan lighthouse are presented in figure 8, figure 9, figure 10 and figure 11. These simulations have been performed considering the sphere approximation algorithm and a 15 minute time-step.

Figure 12 shows the variation of the distance between reflected points and receiver, as a function of the satellite elevation angle, and for several receiver heights above the reflecting surface and figure 13 shows the variation of the area of the first Fresnel surface. Such figures have been produced by doing simulations on the Cordouan lighthouse and varying the receiver height above the reflecting surface. The map of the reflected points obtained for a big receiver height above the reflecting surface will in fact be the same as the one obtained for a smaller receiver height, but more stretched. Henceforth, the higher the receiver height, the bigger the "measurable" area, but the less dense the ground coverage of the data (less reflection points per surface unit).

Assessment of the ocean tide influence

Simulations in the Cordouan lighthouse have been achieved integrating ocean tide from the tide gauge in Royan, by time-varying the receiver height above the sea surface in order to simulate the tide. The vertical visibility mask was set to 10-90°, in order to avoid the weaker accuracy of determination of the specular reflection points positions for satellites with low elevation angle, as highlighted in paragraph 4.4.2. By comparing the results with simulations made with a fixed-receiver height of 60 meters above the sea surface, it appears that the 3D offsets reach values higher than 12 meters for the maximum tide values (< 3 meters) (figure 14). We can expect even higher discrepancies by taking into account satellites whose elevation angle would be lower than 10°.

4.4.2 Geneva Lake

Three sets of simulation have been performed in the case of the Geneva Lake shore, for a 24-hour experiment, on the 4^{th} october 2012:

- first configuration considering a receiver height of 5 meters above lake level
- second configuration considering a receiver height of 50 meters above lake level
- third configuration considering a receiver height of 300 meters above lake level as for an airborne experiment (e.g. hovering helicopter).

Each series has been computed using the four algorithms of determination of the reflection points (local planimetric approximation, local sphere approximation, ellipsoid approximation and the algorithm taking a DEM into account). Results are presented on tables 2 to 7. They show the distances between the specular points and the receiver (arc lengths), and the differences between the positions given by each algorithm. The local sphere approximation have been chosen as reference to be compared with other algorithms given that it is the one the most commonly adopted by the scientific community.

Influence of the receiver height above the reflecting surface

It appears that both planimetric and altimetric differences between the method used increase with the receiver height above the reflecting surface. This is explainable by the fact that the higher the receiver is, the farther the reflection points will be from the receiver, and the bigger the impact of the Earth approximation will be. For a 5-meter receiver height, reflection occurs until approximately 60 meters from the receiver, whereas for a 300-meter receiver height, it occurs until 3400 meters (6700 m when integrating the DEM). It means that, in the second case, reflections occur in the mountains in the South of the receiver hence big differences between the sphere algorithm and the algorithm taking the DEM into account. For a 5 m receiver height above the reflecting surface and considering satellites with elevation angles above 5°, mean planimetric (resp. altimetric) differences are below 11 cm (resp. 2 cm) between the local sphere and ellipsoid approximation and are negligible between the sphere and plane approximations. With a 300 m receiver height above the reflecting surface, mean planimetric (resp. altimetric) differences reach 7.70 m (resp. 1.19 m) between the local sphere and ellipsoid approximation and 2.1 m (resp. 8 cm) between the local sphere and plane approximations.

Influence of the satellite elevation angle

Secondly, by plotting the differences as functions of the satellite elevation angles, we can observe that the lapses between the different algorithms vary in an inversely proportional way than the satellite elevation angle (and so, proportionally to the point distance from the receiver). That is why we re-ran the simulations, putting a more restrictive mask of visibility, tolerating only satellites whose elevation angle is between 10° and 90°. Tables 5, 6, 7 show results we obtain by applying such a mask. The lower the satellite elevation angle is, the farther the specular reflection points from the receiver and the bigger the impact of the Earth approximation is. The choice of the algorithm used to perform the simulations becomes thus really important for the farthest reflection points (i.e for low satellite elevation angles, and high receiver height above the reflecting surface). For example, mean planimetric (resp. altimetric) differences between the local sphere and ellipsoid approximation with a 50 m receiver height are about 1.20 m (resp. 19 cm) considering satellites with elevation angles above 5° and are about 64 cm (resp. 13 cm) considering only satellites with elevation angles above 10°. Mean planimetric differences between the local sphere and plane approximation with a 50 m receiver height are about 6 cm considering the satellites with elevation angles above 5° and are about 2 cm considering only the satellites with elevation angles above 10°. Altimetric differences are negligible in both cases.

Influence of the DEM integration

Integrating a DEM has deleted 245 specular reflection points out of the 905 points determined during 24 hours the 4^{th} of October 2012 with the sphere approximation algorithm (figure 15a). These 245 points came from a wave emitted by a satellite hidden by a mountain located in the south part of the area. In the north part, any reflection point is valid when taking a DEM into account, because in that direction, the relief is flat over the Geneva Lake, and so, satellites are all visible and reflections are possible (figure 15b). Moreover, the points positions have been rectified while taking a DEM into account, since the others algorithms consider that reflections occur (in first approximation) in a plane around the projection of the receiver and without integrating the problem of the presence of relief.

Comparison between algorithms

For a 5-meter receiver height, and for satellite elevations greater than 10°, the mean planimetric difference (resp. altimetric) between the ellipsoid and the sphere algorithm is equal to 5 cm (resp. 1 cm) whereas for a 300-meter receiver height it is equal to 3.81 m (resp. 75 cm). The approximation done by considering the Earth as a sphere or as an ellipsoid does not really affect the precision of the specular reflection point determination when reflection does not occur too far from the receiver (maximum equal to 48 cm (resp. 9 cm) for a distance lower than 28 m) i.e. for low receiver height and high satellite elevation. When reflections occur far from the

receiver, the choice of the approximation begins to be important.

Concerning the algorithm taking the DEM into account, the differences obtained with respect to the sphere or ellipsoid algorithms are quite big even if the specular reflection point is close enough from the receiver. For instance, the mean difference between the sphere algorithm and the one integrating the DEM is bigger than 2.3 m (resp. 9.22 m) for a 5-meter receiver height, and bigger than 92 m (resp. 37 m) for a 300-meter receiver height, and with satellite elevation angle above 5°.

Tropospheric error

Given the geometric configuration of the satellite, the reflection point and the receiver, the same elevation angle correction will have a different effect according to the receiver height above the reflecting surface. It turns out that considering a same satellite at a given time, the corresponding reflection point will be farther for a big receiver height above the reflecting surface than for a smaller one. Consequently, for the same elevation angle correction, the resulting correction of the reflection point position will be higher in the first case than in the second one. Figure 16 shows the differences, in terms of geometric distances, between the reflection points positions obtained with and without taking the tropospheric correction into account (delay and bending) and for different receiver heights. It appears that for low satellite elevation angle and high receiver height, the tropospheric error has a non-negligible influence on the specular point positions (116 m (resp. 32 cm) for a 300-meter receiver height, satellites elevation angle lower than 10°).

Calculation time

An assessment of the simulator performance has been achieved in terms of computation time from runs computed with a computer with 8 Go RAM, intel Core i5-3570 CPU @ 3.40 GHz.

The different series of simulations have been processed with receiver heights of respectively 5, 10, 30, 50, 100, 300 and 500 meters and during 24 hours, the 4^{th} of October 2012. Each series has been processed 10 times and averaged and with the four different algorithms.

Total calculation time to compute the whole day of simulation is between 2 and 3 minutes for the local plane, local sphere and ellispoid approximations and is about ten times longer when integrating a DEM. A big part of the calculation time is due to the conversion from ellipsoidal heights to altitudes (interpolation from a grid) and the creation of the kml files. The receiver height does not really affect calculation time for the fourth algorithm, even for the ellipsoid approximation algorithm and the one integrating a DEM, thanks to the dichotomous process. It is worth reminding that calculation time will highly be influenced by both the capacities of the processor used to do the calculations, and the chosen parameters to reach a precise estimate of position (notably in terms of convergence criteria and tolerances).

5 Conclusions

In this paper, we presented a simulator based on real GNSS satellite ephemeris, as a user-friendly tool, for modelling the trajectories of GNSS electromagnetic waves that are reflected on the surface of the Earth and therefore preparing GNSS-R campaigns more efficiently. The originality of this simulator remains mainly in the integration of a DEM and of the tropospheric error correction. The results of simulations led us to a better understanding of the influence of some parameters on the reflection geometry, namely by quantifying the impact of the receiver height but also the influence of the satellite elevations, the natural relief (DEM), and the troposphere perturbation.

The different simulations realized near to quite rugged topography lead us to the following conclusions:

- the DEM integration is really important for mountainous areas: planimetric differences as arc length (resp. altimetric differences as ellipsoid height) can reach 5.4 km (resp. 1.0 km) for a 300-meter receiver height, considering satellite with elevation angle greater than 10°.
- differences between sphere and ellipsoid approximation are negligible for specular reflection points close from the receiver (closer than 40-50 meters) i.e. small receiver height and/or high satellites elevations. For instance, planimetric differences (resp. altimetric) are smaller than 50 cm (resp. 10 cm) for a 5-meter receiver-height, considering satellites with elevation angle greater than 10°.
- the tropospheric error correction can be negligible with regards to the position of the specular reflection point when the receiver height is below 5 meters, but is absolutely mandatory otherwise, particularly for satellites with low elevation angle where the correction to apply is exponential.

Globally, it is worth reminding that the farther the specular reflection point from the receiver is, the more important the influence of the different error sources will be: Earth approximation, DEM integration, tropospheric error correction. The farthest specular reflection points will be obtained for high receiver height and low satellite elevation. This simulator is likely to be of great help for the preparation of *in situ* experiments involving the GNSS-R technique. Further developments of the simulator will be soon implemented, such as receiver installed on a moving platform in order to map the area covered by airborne GNSS-R measurements campaigns and on-board a LEO satellite.

Acknowledgements. This work was funded by CNES in the framework of the TOSCA project "Hydrologie, Océanographie par Réflectométrie GNSS (HORG)". Nicolas Roussel is supported by a PhD granted from the French Ministère de l'Enseignement Supérieur et de la Recherche (MESR).

References

Beckmann P., Spizzichino A.: Scattering of Electromagnetic Waves from Rough Surfaces. Artech House Publishers. 1987. ISBN 0-89006-238-2.

Billich A.L.: Improving the Precision and Accuracy of Geodetic GPS: Applications to Multipath and Seismology. PhD. B.S., University of Texas at Austin. M.S., University of Colorado. 2004.

Boehm J., Niell A., Tregoning P., Schuh H.: Global Mapping Function (GMF): A new empirical mapping function based on numerical weather model data. Geophysical Research Letters. DOI: 10.1029/2005GL025546. Volume 33, Issue 7, April 2006

Boehm J., Werl B., Schuh H.: Troposphere mapping functions for GPS and very long baseline interferometry from European Centre for Medium-Range Weather Forecasts operational analysis data. Journal of Geophysical Research: Solid Earth 111(B2), doi:10.1029/2005JB003629. 2006.

Cardellach E., Fabra F., Rius A., Pettinato S., Daddio S.: Characterization of Dry-snow Sub-structure using GNSS Reflected Signals, Remote Sensing Environment, 124, pp. 122-134, 2012.

Chen G., Herring T.: Effects of atmospheric azimuthal asymmetry on the analysis of space geodetic data. Journal of Geophysical Research: Solid Earth. DOI: 10.1029/97JB01739. Volume 102, Issue B9, pages 20489–20502, 10 September 1997.

Gegout P., Biancale R., Soudarin L.: Adaptive Mapping Functions to the azimuthal anisotropy of the neutral atmosphere. J. Geodesy., 85, 661-667, 2011.

Gleason S.: Remote Sensing of Ocean, Ice and Land Surfaces Using Bistatically Scattered GNSS Signals From Low Earth Orbit. Thesis (Ph.D.), University of Surrey, 2006. .

Gleason S., Lowe S. Zavorotny V.: Remote sensing using bistatic GNSS reflections. GNSS applications and methods, 399-436, 2009.

Helm A.: Ground based GPS altimetry with the L1 openGPS receiver using carrier phase-delay observations of reflected GPS signals. Thesis (Ph.D.), Deutsches GeoForschungsZentrum (GFZ), 164 pp, 2008.

Hobiger T., Ichikawa R., Takasu T., Koyama Y., Kondo T.: Ray-traced troposphere slant delays for precise point positioning. Earth Planets Space, 60, e1–e4, 2008.

Jarvis J., Reuter H., Nelson A., Guevara E.: Hole-filled SRTM for the globe. CGIAR-CSI SRTM 90 m DAtabase, Version 4. CGIAR Consort. for Spatial Inf.,2008.

Katzberg S., Torres O., Grant M.S., Masters D.: Utilizing calibrated GPS reflected signals to estimate soil reflectivity and dielectric constant: results from SMEX02. Remote Sensing of Environment 100 (1), 17-28, 2006.

Komjathy A., Zavorotny V., Axelrad P., Born G., Garrison J.: GPS signal scattering from sea surface. Wind speed retrieval using experimental data and theoretical model. Remote Sensing of Environment 73, 162–174, 2000.

Kostelecky J., Klokocnik J., Wagner C.A.: Geometry and accuracy of reflecting points in bistatic satellite altimetry. J Geod (2005) 79: 421-430. DOI: 10.1007/s00190-005-0485-7, 2005.

Lagler K., Schindelegger M., Boehm J., Krsn H., Nilsson T. GPT2: Empirical slant delay model for radio space geodetic techniques. Geophysical Research Letters 40(6):1069–1073, doi:10.1002/grl.50288. 2013.

Larson K.M., Nievinski F.G.: GPS snow sensing: results from the EarthScope Plate Boundary Observatory. GPS Solut. 17:41-52, DOI 10.1007/s10291-012-0259-7, 2013.

Löfgren J.S., Haas R., Johansson J.: High-rate local sea level monitoring with a GNSS-based tide gauge. IGARSS 2010, Page range: 3616-3619, DOI: 10.1109/IGARSS.2010.5652888, 2010.

Löfgren J.S., Rüdiger H. Scherneck H.G.: Sea-Level analysis using 100 days of reflected GNSS signals. Proceedings of the 3rd International Colloquium - Scientific and Fundamental Aspects of the Galileo Programme, 31 August - 2 September 2011, Copenhagen, Denmark, (WPP 326) pp. 5, 2011.

Lowe S.T. Zuffada C., Chao Y., Kroger P., Young L.E., LaBrecque J.L.: 5-cm-Precision aircraft ocean altimetry using GPS reflections, GEOPHYSICAL RESEARCH LETTERS, VOL. 29, NO. 10, 1375, doi: 10.1029/2002GL014759, 2002.

Marini J.W.: Correction of satellite tracking data for an arbitrary tropospheric profile. Radio Sci 7(2):223-231. doi:10.1029/RS007i002p00223, 1972.

Martin-Neira M.: A passive reflectometry and interferometry system (PARIS): Application to ocean altimetry. ESA J-EUR SPACE AGEN, Vol. 17, 331-355, 1993.

Nafisi, V., Urquhart L., Santos M.C., Nievinski F.G., Bohm J., Wijaya D.D., Schuh H., Ardalan A.A., Hobiger T., Ichikawa R., Zus F., Wickert J., Gegout P.: Comparison of Ray-Tracing Packages for Troposphere Delays. Geoscience and Remote Sensing. Volume 50 Issue 2. 2012, Page range: 469 - 481, DOI: 10.1109/TGRS.2011.2160952.

NASA and NIMA: The Development of the Joint NASA GSFC and the National Imagery and Mapping Agency (NIMA) Geopotential Model EGM96. NASA/TP-1998-206861. 1998.

Niell A.: Preliminary evaluation of atmospheric mapping functions based on numerical weather models. A.E. Niell. Proceedings of the First COST Action 716 Workshop Towards Operational GPS Meteorology and the Second Network Workshop of the International GPS Service (IGS).Volume 26, Issues 6–8, 2001, Pages 475–480

Nievinski F.G.: Ray-tracing options to mitigate the neutral atmosphere delay in GPS, thesis (Ph.D.), 255 p., 2009.

NIMA: National Imagery and Mapping Agency: Departement of Defense Wolrd Geodetic System 1984. NIMA Stock No. DMATR83502WGS84. NSN 7643-01-402-0347. 1997.

Nocedal J., Wright S.J.: Numerical Optimization, Springer. ISBN 978-0-387-30303-1, 2006, Place of publication: USA (TB/HAM).

Rius A., Aparicio J.M., Cardellach E., Martin-Neira M., Chapron B.: Sea surface state measured using GPS reflected signals. Geophysical Research Letters 29 (23), doi:10.1029/2002GL015524, 2002.

Rius A., Noque's-Correig O., Ribo S., Cardellach E., Oliveras S., Valencia E., Park H., Tarongi J.M., Camps A., Van Der Marel H., Van Bree R., Altena B., Martin-Neira M.: Altimetry with GNSS-R interferometry: first proof of concept Experiment, GPS Solutions(16), 231-241, DOI 10.1007/s10291-011-0225-9, 2012.

Rodriguez E., Morris C.S., Belz J.E., Chapin E.C., Martin J.M., Daffer W., Hensley S.: An assessment of the SRTM topographic products. Technical Report D-31639, JPL/NASA,2005.

Rodriguez-Alvarez N., Bosch-Lluis X., Camps A., Vall-Llossera M, Valencia E., Marchan-Hernandez J.F., Ramos-Perez I.: Soil moisture retrieval using GNSS-R techniques: Experimental results over a bare soil field. IEEE Trans. Geosci. Remote Sens., vol. 47, no. 11, pp. 3616–3624, 2009.

Rodriguez-Alvarez N., Camps A., Vall-Llossera M, Bosch-Lluis X., Monerris A., Ramos-Perez I. Valencia E., Marchan-Hernandez J.F., Martinez-Fernandez J., Baroncini-Turricchia G., Pérez-Gutiérrez C., Sanchez N.:Land Geophysical Parameters Retrieval Using the Interference Pattern GNSS-R Technique, IEEE TRANSACTIONS ON GEOSCIENCE AND REMOTE SENSING, VOL. 49, NO. 1, 71-84, 2011.

Ruffini G., Soulat F., Caparrini M., Germain O., Martin-Neira M.: The Eddy Experiment: Accurate GNSS-R ocean altimetry from low altitude aircraft, Geophys. Res. Lett., 31, L12306, doi:10.1029/2004GL019994. 2004.

Semmling A.M, Beyerle G., Stosius R., Dick G., Wickert J., Fabra F., Cardellach E., Ribo S., Rius A., Helm A., Yudanov S.B., d'Addio S.: Detection of Arctic Ocean tides using interferometric GNSS-R signals. Geophysical Research Letters, 38, L04103 DOI 10.1029/2010GL046005. 2011.

Soulat F., Caparrini M., Germain O., Lopez-Dekker P., Taani M., and Ruffini G.: Sea state monitoring using coastal GNSS-R, Geophys. Res. Lett., 31, L21303, doi 10.1029/2004GL020680. 2004.

Treuhaft P., Lowe S., Zuffada C., Chao Y.: 2-cm GPS altimetry over Crater Lake, GEOPHYSICALR ESEARCHL ETTERS,VOL. 28, NO. 23, PAGES 4343-4436.2004.

Wagner C., Klokocnik C.: The value of ocean reflections of GPS signals to enhance satellite altimetry: data distribution and error analysis. Journal of Geodesy (2003) 77: 128-138. DOI: 10.1007/s00190-002-0307-0, 2003.

Zavorotny A.U., Voronovich A.G.: Scattering of GPS signals from the ocean with wind remote sensing application. IEEE Transactions on Geosciences and Remote Sensing 38 (2), 951–964, 2000.

Zus F., Bender M., Deng Z., Dick G., Heise S., Shang-Guan M., Wickert J.: A methodology to compute GPS slant total delays in a numerical weather model. Radio Science. DOI: 10.1029/2011RS004853.Volume 47, Issue 2, April 2012.

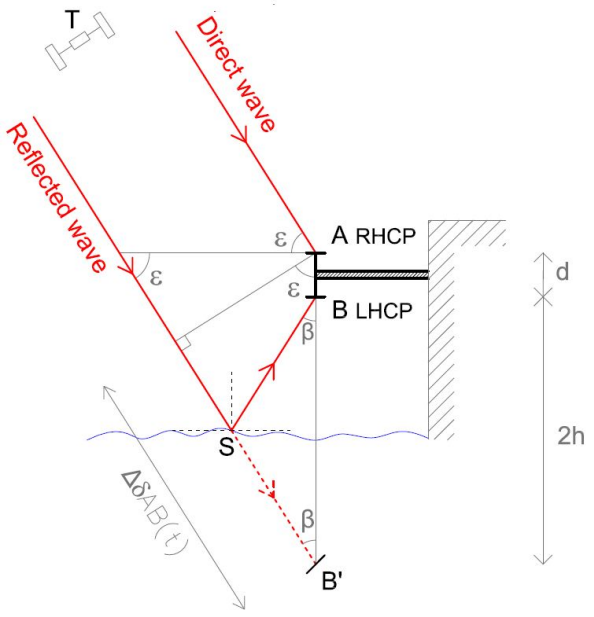

Fig. 1. Principle of GNSS-Reflectometry.
T: satellite/transmitter, S: specular reflection point, ϵ: satellite elevation, $\triangle\ \delta AB(t)$: additional path covered by the reflected wave, d : interdistance between the LHCP and RHCP antennas and h: height of the receiver above the reflecting surface.

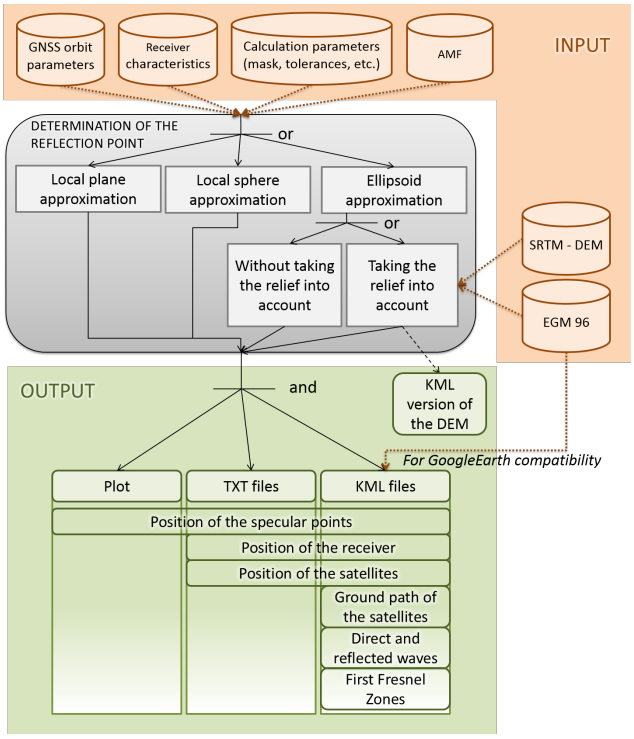

Fig. 2. Data flow chart of the simulator.
Three main blocks: an input block which contains the different elements mandatory for the processing; a processing block where the user can choose which algorithm to be used, and an output block containing the different results of the simulation, namely KML files to be opened with Google Earth.

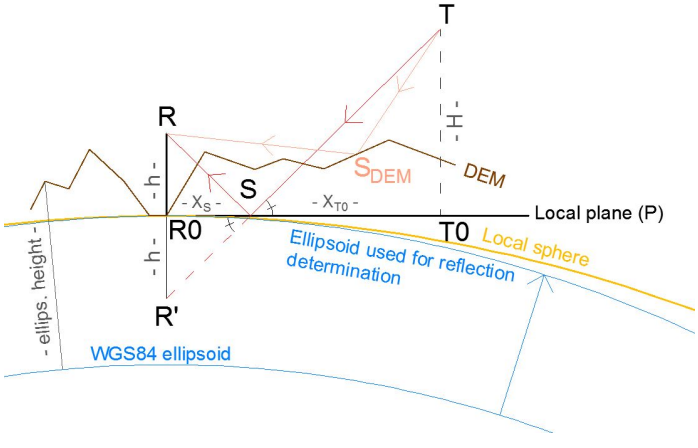

Fig. 3. Determination of the specular reflection point in a local plane approximation and local difference with the sphere and ellipsoid approximations and DEM integration.
S: specular reflection point position. R: receiver position. T: transmitter/satellite position. h: height of the receiver above the ground surface.

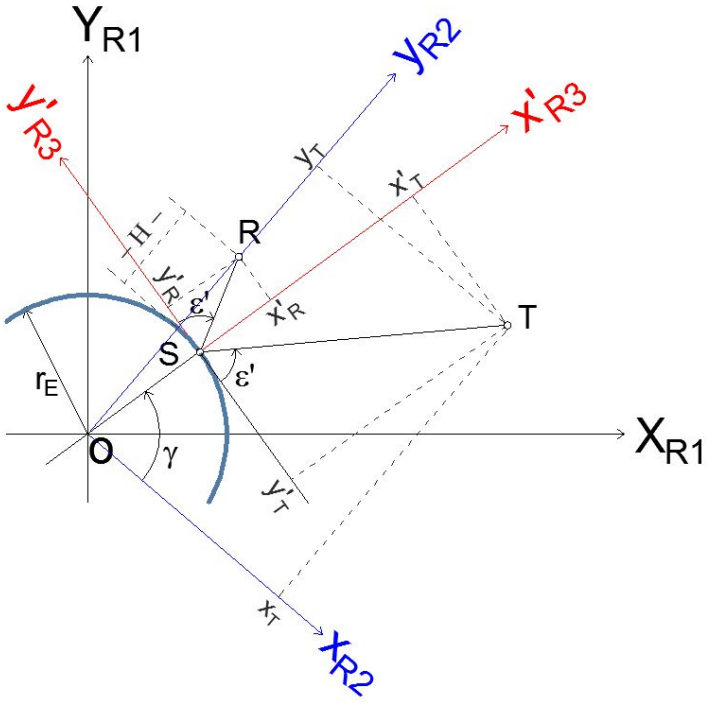

Fig. 4. Local sphere approximation : the three different reference systems of coordinates.
S: specular reflection point position. R: receiver position. T: transmitter/satellite position. $(0, X, Y, Z)_{R1}$: WGS84 Cartesian system. $(0, x, y)_{R2}$: local two-dimensional system, obtained by the rotation of the R1 system around the Z axis, in such a way that $x_r = 0$. $(S, x', y')_{R3}$: a local two-dimensional system, obtained by a rotation around the z axis and a r_R translation of the R2 system in such a way that x' and the local vertical are colinear and that the system origin coincides with the specular reflection point S.

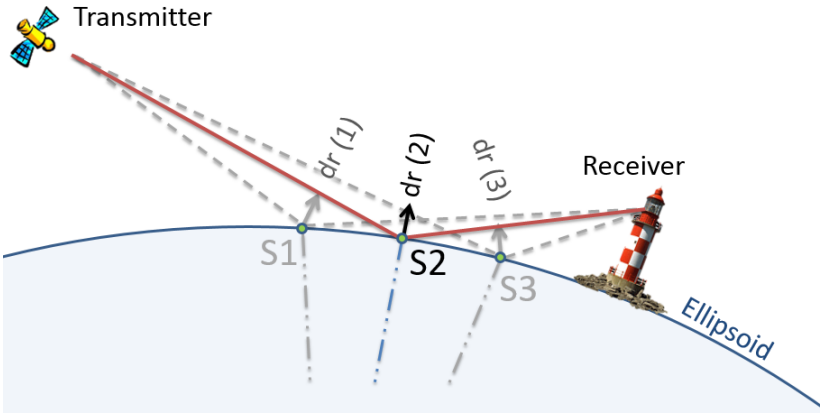

Fig. 5. Local ellipsoid approximation.
S2: specular reflection point position. S1, S3: temporary positions of the specular reflection point before convergence. Let dr be the sum of the normalized anti-incident and scattering vector (i.e. the bisecting vector). In the specular reflection point position, dr is colinear with the local vertical. We apply a dichotomous process until having this condition verified.

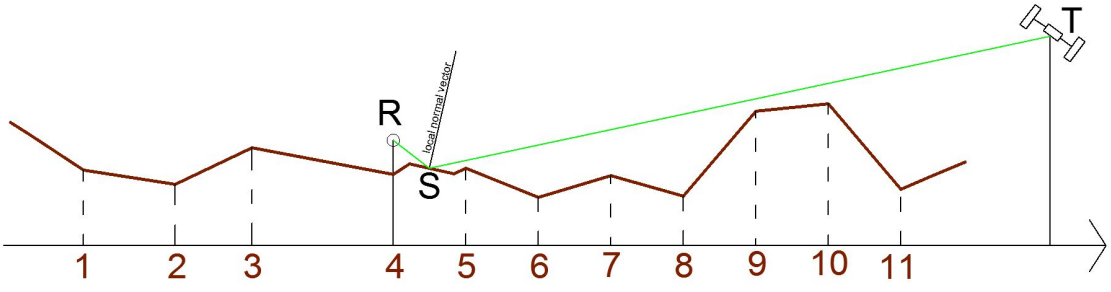

Fig. 6. Determination of the specular reflection point integrating a DEM
S: specular reflection point position. R: receiver position. T: transmitter/satellite position. A dichotomous process is applied for each topographic segment of the DEM to find if there is a point where the bisecting angle (equal to the sum of the anti-incident and scattering vectors) is colinear with the local normal vector.

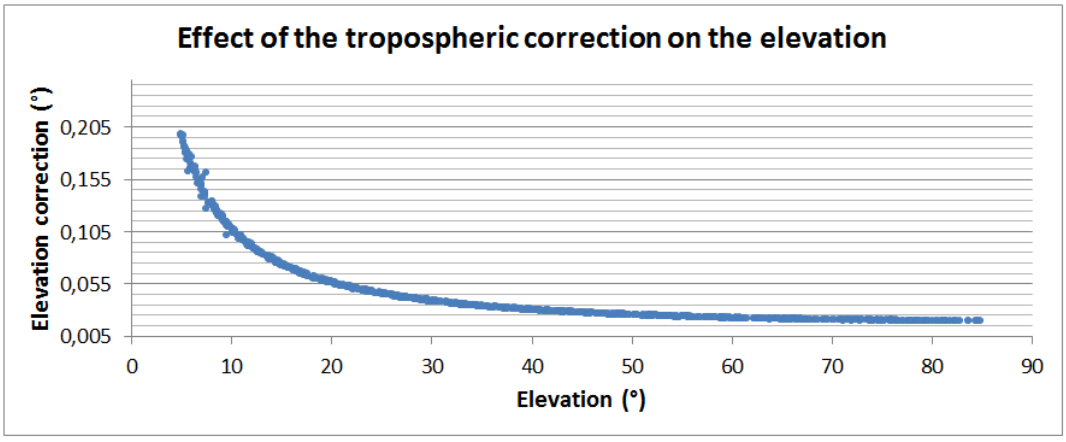

Fig. 7. Effect of the neutral atmosphere on the elevation angle.
An exponential correction must be made for satellites with low elevation angle.

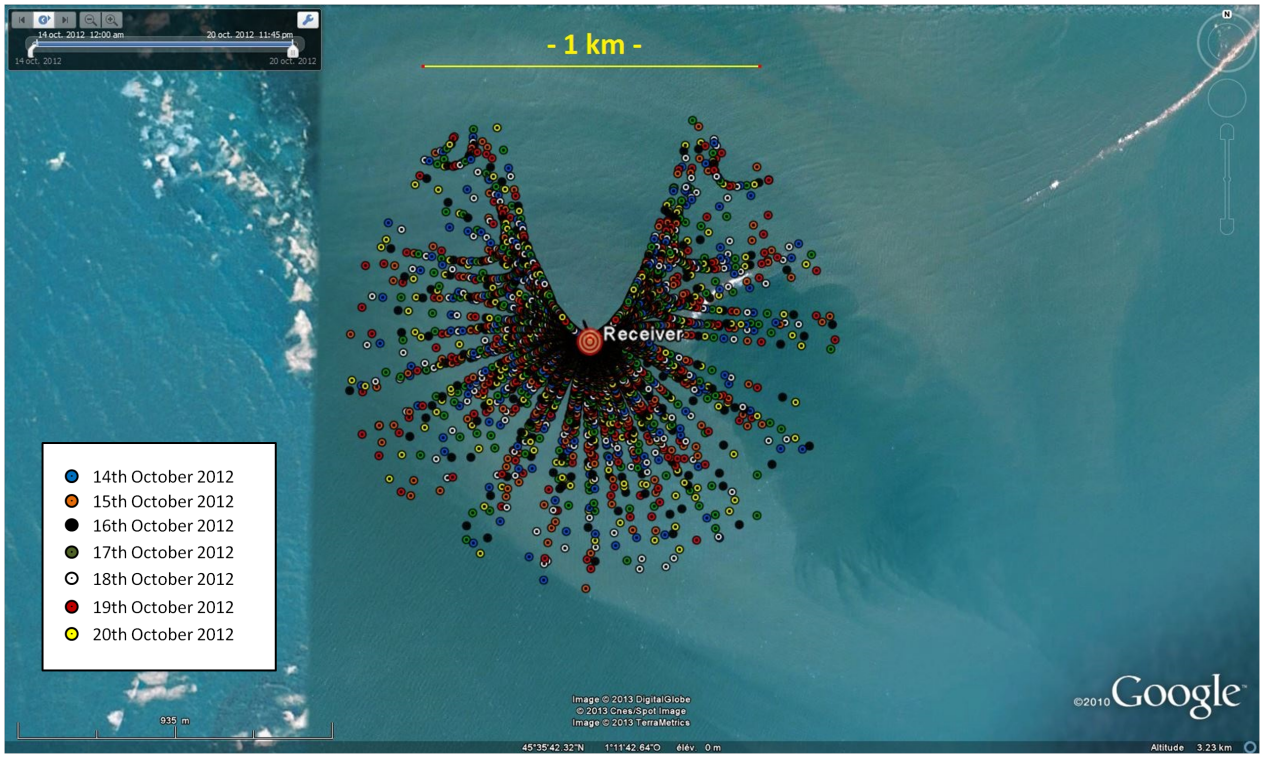

Fig. 8. Positions of the specular reflection points for one week of simulation on the Cordouan lighthouse with a 15 minutes sampling rate (i.e. satellites positions actualized each 15 minutes).
Note the gap in the North direction.

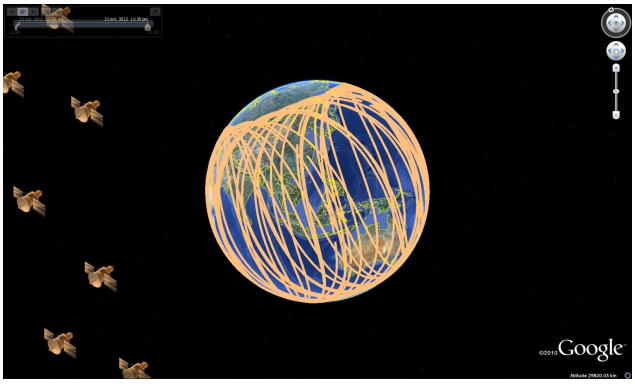

Fig. 9. Ground tracks of the GPS satellites the 4^{th} October 2012.

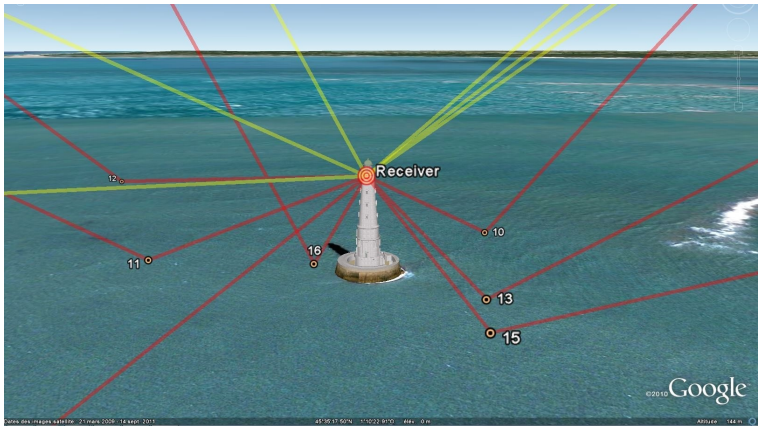

Fig. 10. Direct and reflected waves display: Cordouan lighthouse simulation.

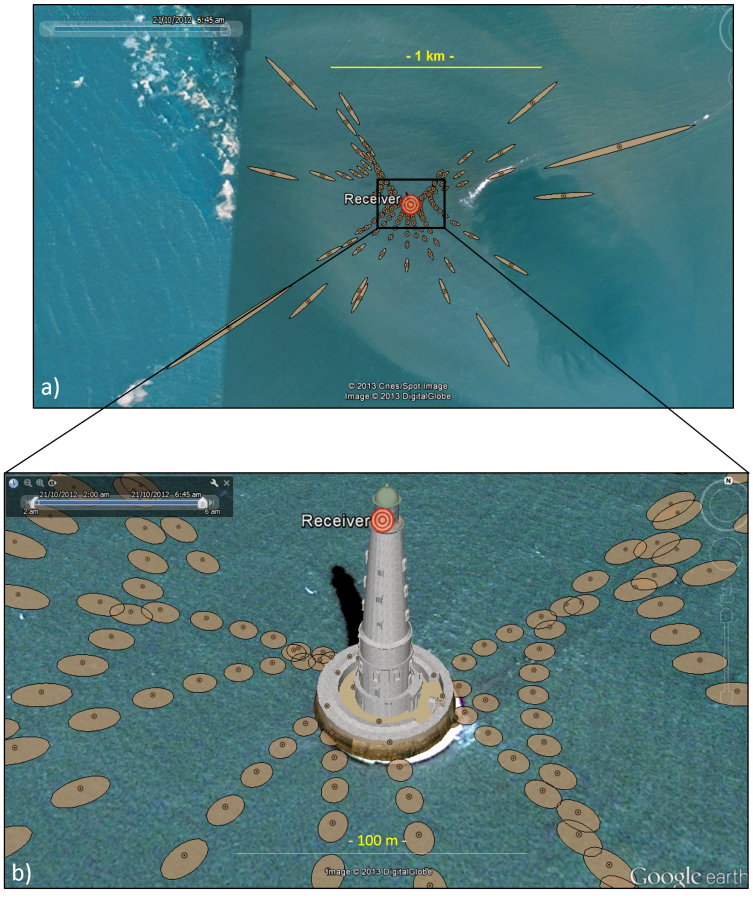

Fig. 11. First Fresnel surfaces distribution
a) global point of view with a radius close to 1 km; b) zoom centered on the Cordouan lighthouse.

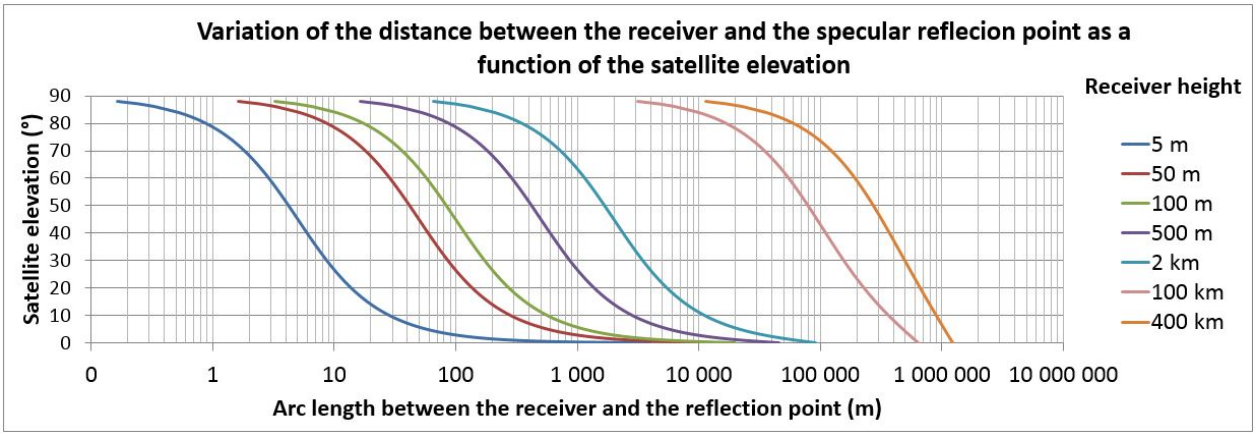

Fig. 12. Variation of the distance between the receiver and the specular reflection point, as a function of the satellite elevation, for different receiver heights.

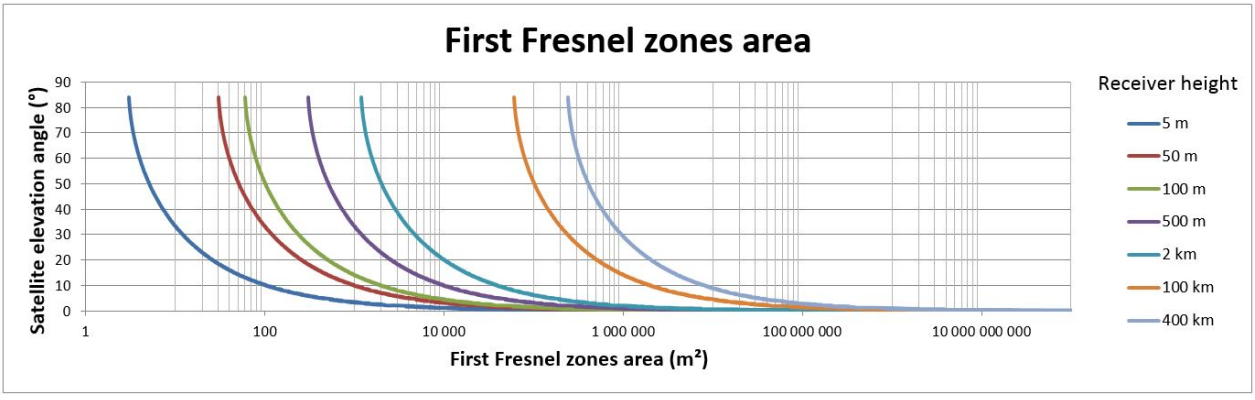

Fig. 13. First Fresnel surface area as a function of the satellite elevation, for different receiver heights.

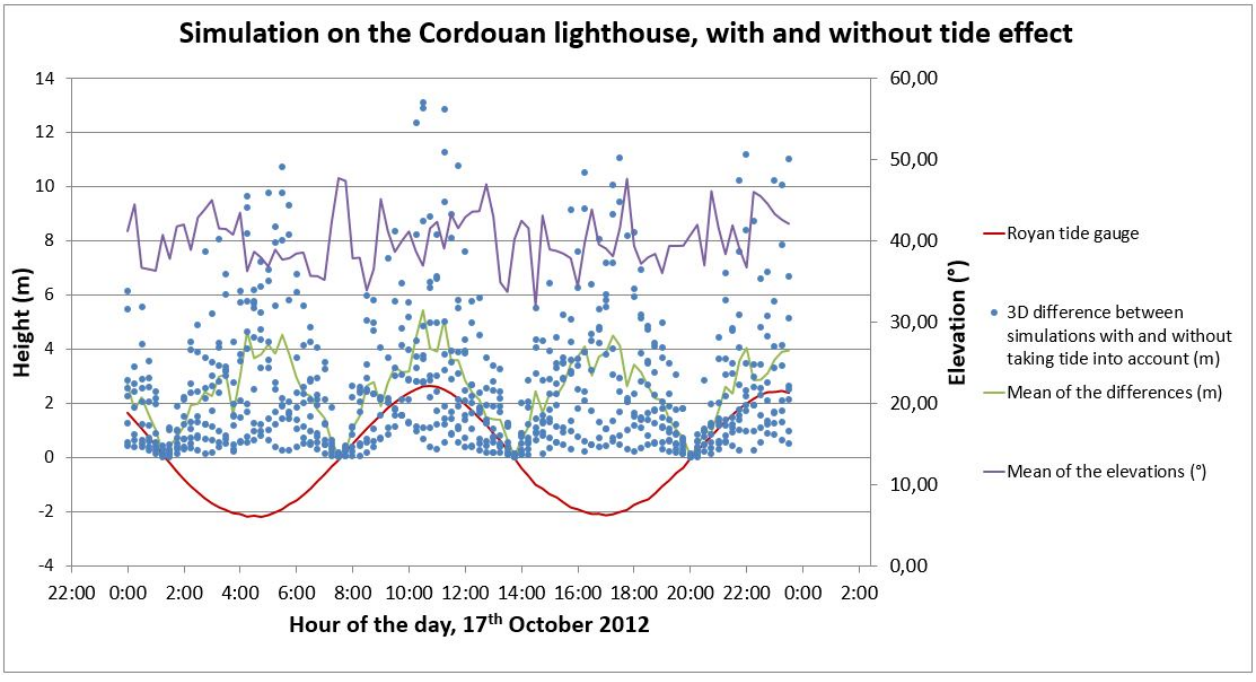

Fig. 14. Assessment of the tide influence.
The red line shows the tide from the Royan tide gauge and must be linked with the left vertical axis. The blue dots (resp. green line) are the 3D differences (resp. mean of the 3D differences) between simulations with and without taking the tide into account (i.e. taking the mean sea level over the period as reference) and must also be read with the left vertical axis. The purple line must be read with the right vertical axis and shows the mean of the satellite elevation angles. The impact of the tide on the size of the reflecting area is non-negligible (decametric 3D-differences), and it is worth noticing that the gaps would have been even bigger integrating satellites with low elevation angle. Note also the fact that the periodic variations of the 3D variations are only linked to the tide, since the mean of the satellite elevation angles does not show periodic variation during the day of simulation.

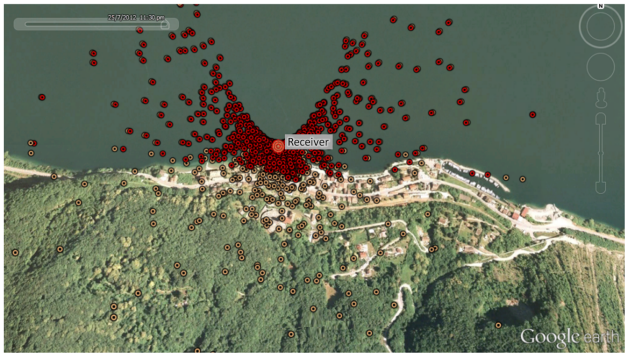

Fig. 15a. Influence of the relief - Specular reflection points on the shore of the Geneva lake (46°24'30N";6°43'6"E).
Red dots: sphere approximation algorithm (altitudes have been increased so that all the points be visible) Orange dots: taking a DEM into account

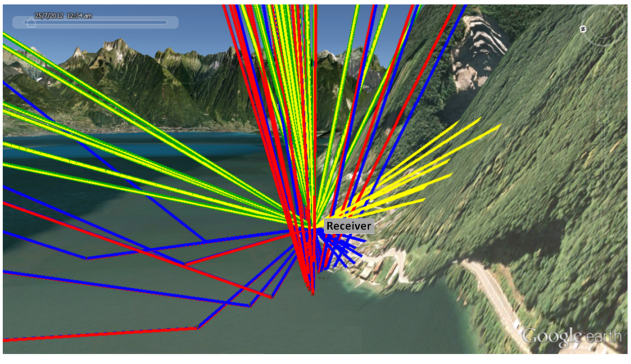

Fig. 15b. Influence of the relief - Direct and reflected waves display. (Relief amplifier by a factor 3) Yellow lines: direct waves, sphere approximation algorithm ; Green lines: direct waves, taking a DEM into account ; Blue lines: reflected waves, sphere approximation algorithm ; Red lines: reflected waves, taking a DEM into account. It is noticeable that some yellow and blue lines (direct and reflected waves, sphere approximation algorithm) go through the moutain (reflection points having been calculated *inside* the moutain), whereas any red or green line (direct and reflected waves, intergrating a DEM) go through it.

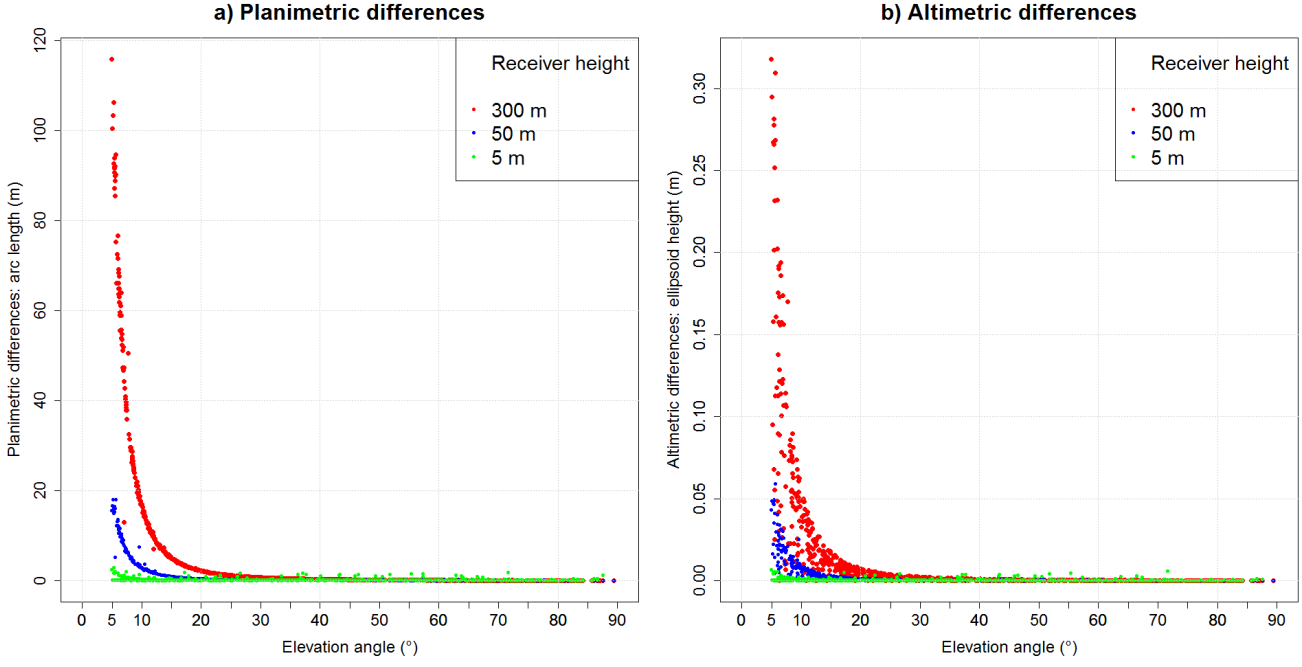

Fig. 16. Importance of tropospheric correction versus elevation and receiver height with respect to reflecting surface height.
a) Planimetric differences as arc length (m). b) Altimetric differences as ellipsoid height (m).

Table 1. Cross-validation between ellipsoid approximation and DEM integration

		Receiver height (m)		
		5	50	300
Distance to the specular reflection point with respect to the receiver: arc length (m)	Mean	13	122	730
	Maximum	58	573	3408
Position differences (m) (planimetric / altimetric)	Mean	**0.007/0**	**0.008/0**	**0.04/0**
	Maximum	0.1/0	0.1/0	0.7/0

Table 2. Position differences (arc length and 3D geometric distance) between the different algorithms. Height: 5 m, elevation $> 5°$.

Vertical visibility mask (°)		**5 - 90**					
Horizontal visibility mask (°)		0 - 360					
Receiver height (m)		**5**					
Algorithm		Sphere	Plane	Sphere	Ellipsoid	Sphere	DEM
Distance with respect to the receiver: arc length (m)	Minimum	0.23	0.23	0.23	0.23	0.23	0.21
	Maximum	57.32	57.33	57.32	55.56	57.32	66.98
	Mean	11.30	11.30	11.30	11.26	11.30	12.95
	Standard deviation	11.59	11.59	11.59	11.47	11.59	13.65
Propagation difference (m)	Minimum	0.87	0.87	0.87	0.87	0.87	0.00
	Maximum	9.99	9.99	9.99	9.99	9.99	0.59
	Mean	5.68	5.69	5.68	5.68	5.68	0.13
	Standard deviation	2.81	2.81	2.81	2.81	2.81	0.12
Planimetric differences (m) (cartesian WGS84 / geodesic arc-length)	Minimum	0.00/0.00		0.02 / 0.00		3.12 / 0.00	
	Maximum	0.01 / 0.00		1.44 / 1.81		22.96 / 20.94	
	Mean	**0.00 / 0.00**		**0.10 / 0.11**		**6.67 / 2.25**	
	Standard deviation	0.00 / 0.00		0.19 / 0.25		1.57 / 1.99	
Altimetric differences (m) (cartesian WGS84 / geodesic arc-length)	Minimum	0.00/0.00		0.02 / 0.00		4.84 / 8.74	
	Maximum	0.01 / 0.01		1.24 / 0.17		10.29 / 10.86	
	Mean	**0.00 / 0.00**		**0.08 / 0.02**		**6.82 / 9.22**	
	Standard deviation	0.00 / 0.00		0.15 / 0.03		0.92 / 0.41	

Table 3. Position differences (arc length and 3D geometric distance) between the different algorithms. Height: 50 m, elevation $> 5°$.

Vertical visibility mask (°)		**5 - 90**					
Horizontal visibility mask (°)		0 - 360					
Receiver height (m)		**50**					
Algorithm		Sphere	Plane	Sphere	Ellipsoid	Sphere	DEM
Distance with respect to the receiver: arc length (m)	Minimum	2.21	2.21	2.21	2.05	2.21	0.19
	Maximum	572.38	573.28	572.38	554.84	572.38	6678.56
	Mean	104.32	104.36	104.32	103.66	104.32	527.53
	Standard deviation	111.69	111.79	111.69	109.91	111.69	553.92
Propagation difference (m)	Minimum	8.67	8.66	8.67	8.94	8.67	102.09
	Maximum	99.91	99.91	99.91	99.92	99.91	763.27
	Mean	59.44	59.44	59.44	59.46	59.44	368.01
	Standard deviation	27.80	27.80	27.80	27.75	27.80	149.11
Planimetric differences (m) (cartesian WGS84 / geodesic arc-length)	Minimum	0.00/0.00		0.22 / 0.31		7.02 / 1.87	
	Maximum	0.73 / 1.06		13.51 / 17.99		5391.80 / 5443.61	
	Mean	**0.03 / 0.06**		**0.92 / 1.20**		**101.29 / 90.95**	
	Standard deviation	0.10 / 0.15		1.76 / 2.29		379.44 / 375.87	
Altimetric differences (m) (cartesian WGS84 / geodesic arc-length)	Minimum	0.00/0.00		0.17 / 0.00		0.03 / 4.19	
	Maximum	0.53 / 0.03		12.32 / 1.64		953.09 / 1053.38	
	Mean	**0.02 / 0.00**		**0.77 / 0.19**		**19.28 / 40.07**	
	Standard deviation	0.06 / 0.00		1.51 / 0.27		81.44 / 93.69	

Table 4. Position differences (arc length and 3D geometric distance) between the different algorithms. Height: 300 m, elevation > 5°.

Vertical visibility mask (°)		5 - 90					
Horizontal visibility mask (°)		0 - 360					
Receiver height (m)		300					
Algorithm		Sphere	Plane	Sphere	Ellipsoid	Sphere	DEM
Distance with respect to the receiver: arc length (m)	Minimum	13.26	13.26	13.26	12.32	13.26	0.19
	Maximum	3407.44	3439.29	3407.44	3304.53	3407.44	6678.57
	Mean	660.75	662.36	660.75	656.16	660.75	733.13
	Standard deviation	714.13	717.99	714.13	703.71	714.13	810.51
Propagation difference (m)	Minimum	52.15	51.99	52.15	53.78	52.15	11.88
	Maximum	599.45	599.45	599.45	599.49	599.45	763.28
	Mean	353.16	353.13	353.16	353.40	353.16	335.48
	Standard deviation	172.72	172.75	172.72	172.43	172.72	168.19
Planimetric differences (m) (cartesian WGS84 / geodesic arc-length)	Minimum	0.00/0.00		1.33 / 1.95		7.02 / 1.87	
	Maximum	25.98 / 37.56		79.18 / 105.64		5391.80 / 5443.61	
	Mean	**1.42 / 2.05**		**5.86 / 7.70**		**100.51 / 91.84**	
	Standard deviation	3.88 / 5.62		10.95 / 14.26		378.05 / 375.10	
Altimetric differences (m) (cartesian WGS84 / geodesic arc-length)	Minimum	0.00/0.00		1.02 / 0.00		0.03 / 0.33	
	Maximum	18.70 / 1.02		72.46 / 9.79		953.09 / 1053.38	
	Mean	**0.68 / 0.08**		**5.02 / 1.19**		**20.36 / 36.70**	
	Standard deviation	2.20 / 0.16		9.43 / 1.68		79.98 / 89.66	

Table 5. Position differences (arc length and 3D geometric distance) between the different algorithms. Height: 5 m, elevation > 10°.

Vertical visibility mask (°)		10 - 90					
Horizontal visibility mask (°)		0 - 360					
Receiver height (m)		5					
Algorithm		Sphere	Plane	Sphere	Ellipsoid	Sphere	DEM
Distance with respect to the receiver: arc length (m)	Minimum	0.23	0.23	0.23	0.23	0.23	0.21
	Maximum	27.74	27.75	27.74	27.55	27.74	37.18
	Mean	8.22	8.22	8.22	8.23	8.22	9.12
	Standard deviation	6.54	6.54	6.54	6.53	6.54	7.45
Propagation difference (m)	Minimum	1.77	1.77	1.77	1.78	1.77	0.00
	Maximum	9.99	9.99	9.99	9.99	9.99	0.59
	Mean	6.15	6.15	6.15	6.15	6.15	0.14
	Standard deviation	2.54	2.54	2.54	2.54	2.54	0.12
Planimetric differences (m) (cartesian WGS84 / geodesic arc-length)	Minimum	0.00/0.00		0.02 / 0.00		4.36 / 0.00	
	Maximum	0.01 / 0.00		0.41 / 0.48		12.94 / 10.03	
	Mean	**0.00 / 0.00**		**0.06 / 0.05**		**6.70 / 1.80**	
	Standard deviation	0.00 / 0.00		0.05 / 0.08		1.26 / 1.35	
Altimetric differences (m) (cartesian WGS84 / geodesic arc-length)	Minimum	0.00/0.00		0.02 / 0.00		4.91 / 8.91	
	Maximum	0.01 / 0.01		0.33 / 0.09		8.78 / 10.86	
	Mean	**0.00 / 0.00**		**0.04 / 0.01**		**6.62 / 9.25**	
	Standard deviation	0.00 / 0.00		0.04 / 0.02		0.65 / 0.42	

Table 6. Position differences (arc length and 3D geometric distance) between the different algorithms. Height: 50 m, elevation > 10°.

Vertical visibility mask (°)		10 - 90					
Horizontal visibility mask (°)		0 - 360					
Receiver height (m)		50					
Algorithm		Sphere	Plane	Sphere	Ellipsoid	Sphere	DEM
Distance with respect to the receiver: arc length (m)	Minimum	2.21	2.21	2.21	2.05	2.21	0.19
	Maximum	277.34	277.44	277.34	275.42	277.34	6678.56
	Mean	76.38	76.38	76.38	76.27	76.38	527.53
	Standard deviation	63.09	63.10	63.09	62.83	63.09	553.92
Propagation difference (m)	Minimum	17.66	17.66	17.66	17.78	16.66	102.09
	Maximum	99.91	99.91	99.91	99.92	99.91	763.27
	Mean	63.85	63.85	63.85	63.5	63.85	368.01
	Standard deviation	24.91	24.91	24.91	24.88	24.91	149.11
Planimetric differences (m) (cartesian WGS84 / geodesic arc-length)	Minimum	0.00/0.00		0.22 / 0.31		7.02 / 1.87	
	Maximum	0.10 / 0.16		4.08 / 4.79		5391.80 / 5443.61	
	Mean	**0.01 / 0.02**		**0.48 / 0.64**		**101.29 / 90.95**	
	Standard deviation	0.02 / 0.04		0.46 / 0.58		379.44 / 375.87	
Altimetric differences (m) (cartesian WGS84 / geodesic arc-length)	Minimum	0.00/0.00		0.17 / 0.00		0.03 / 4.19	
	Maximum	0.06 / 0.01		3.27 / 0.86		953.09 / 1053.38	
	Mean	**0.00 / 0.00**		**0.42 / 0.13**		**19.28 / 40.07**	
	Standard deviation	0.01 / 0.00		0.40 / 0.14		81.44 / 93.69	

Table 7. Position differences (arc length and 3D geometric distance) between the different algorithms. Height: 300 m, elevation > 10°.

Vertical visibility mask (°)		10 - 90					
Horizontal visibility mask (°)		0 - 360					
Receiver height (m)		300					
Algorithm		Sphere	Plane	Sphere	Ellipsoid	Sphere	DEM
Distance with respect to the receiver: arc length (m)	Minimum	13.26	13.26	13.26	12.32	13.26	0.19
	Maximum	1660.78	1664.57	1660.78	1649.33	1660.78	6678.56
	Mean	453.50	453.83	453.50	452.28	453.50	527.53
	Standard deviation	381.89	382.46	381.89	379.68	381.89	553.92
Propagation difference (m)	Minimum	106.02	105.94	106.02	105.94	106.02	102.09
	Maximum	599.45	599.45	599.45	599.49	599.45	763.27
	Mean	386.56	386.54	386.56	386.71	386.56	368.01
	Standard deviation	152.00	152.02	152.00	151.81	152.00	149.11
Planimetric differences (m) (cartesian WGS84 / geodesic arc-length)	Minimum	0.00/0.00		1.34 / 1.95		7.02 / 1.87	
	Maximum	3.66 / 5.32		18.02 / 26.10		5391.80 / 5443.61	
	Mean	**0.30 / 0.43**		**2.80 / 3.81**		**101.29 / 90.95**	
	Standard deviation	0.59 / 0.86		2.51 / 3.31		379.44 / 375.87	
Altimetric differences (m) (cartesian WGS84 / geodesic arc-length)	Minimum	0.00/0.00		1.02 / 0.00		0.03 / 4.19	
	Maximum	2.22 / 0.23		19.51 / 4.57		953.09 / 1053.38	
	Mean	**0.12 / 0.03**		**2.61 / 0.75**		**19.28 / 40.07**	
	Standard deviation	0.26 / 0.04		2.41 / 0.80		81.44 / 93.69	